Proceedings of the 2011 ASME International Mechanical Engineering Congress & Exposition
IMECE2011
November 11-17, 2011, Denver, Colorado, USA

IMECE2011-63534

A BIOMIMETIC ELASTIC CABLE DRIVEN QUADRUPED ROBOT — THE ROBOCAT

Elvedin Kljuno[♣], J. Jim Zhu[♠], Robert L. Williams II[♣], Stephen M. Reilly[#]

[♣]Mechanical Engineering Department, [♠]School of Electrical Engineering and Computer Science, [#]Biological Sciences Department,
Ohio University, Athens, Ohio 45701, USA

ABSTRACT

State of the art legged robots, such as the Honda's series of bipedal robots ending in the latest advanced walking robot ASIMO, and the series of bipedal robots of Waseda University including the latest advanced robot WABIAN, employ joint-mount motors, which simplifies the analysis/design and traces the route for an effective control system, but results in legs that are heavy and bulky. Cable-driven robots overcome this shortcoming by allowing the motors to be mounted on or near the torso, thereby reducing the weight and inertia of the legs, resulting in lower overall weight and power consumption. To facilitate analysis and design, typical cable-driven robots use non-stretchable cables, which require at least n+1 motors for an n Degree-of-Freedom (DoF) joint. Therefore, for a robot with N joints, at least N additional motors are needed comparing to joint-mount motor drives. Moreover, the drive train of both joint-mount and cable-driven designs are rigid, which cannot effectively absorb ground impact shocks nor transfer potential energy to kinetic energy and vice versa when the robot is in motion, as biologic animals do.

In this paper we present the design and test of a cat-size quadruped robot called RoboCat, which employs stretchable elastic cable-driven joints as inspired by biological quadruped animals. Although it complicates kinematics and dynamics analysis and design, the elastic cables allow n motors to be used for an n-DoF joint, thereby eliminating N motors for a robot with N joints comparing to non-stretchable cables, further realizing the weight and power savings of the cable driven design. Moreover, the elastic cable driven joints not only effectively absorb ground contact shock, but also effectively transfer potential and kinetic energy during walking or running, thereby improving the robot motion performance and energy efficiency. In the paper we will discuss the kinematics and dynamics analysis of elastic cable driven joints, implementation of elastic cable-driven joints on the Ohio University RoboCat, and control.

1. INTRODUCTION

Traditional direct drive actuation system of robotic manipulators is probably one of the easiest ways to actuate robotic walkers, due to its simplicity in mechanical implementation and the fact that the rotational motion of motors is directly mapped into rotational motion of the joints. Consequently, if we just require an appropriate functionality of a robotic walker, the direct drives with a gear set would be a convenient solution. However, biological walkers that use an inverted pendulum like mechanism [1, 2, 3] are considered energy efficient relatively with respect to the state of the art robotic walkers [12, 13], using a different kind of actuators, the muscles, which can be considered as elastic (stretchable) linear actuators. Energy efficiency and the level of the walk cycle precision and smoothness are among important reasons for mimicking biological walkers. As the fundamental actuator unit, the muscle behavior and structure attract special attention of research in robotics. There have been a number of attempts to produce artificial muscles for use in robotics [4 - 8], based on different principles such as pneumatics, piezoelectric effect, magnetostriction, etc.

One of the possibilities of a walking robot muscle-like actuation is to use (elastic) cables. Applications of the cable

[♠]Contact author email: zhuj@ohio.edu

This paper is based on research sponsored by the Air Force Research Laboratory, under agreements number FA8651-07-1-0010 and number FA8651-09-1-0016. The U.S. Government is authorized to reproduce and distribute reprints for Governmental purposes notwithstanding any copyright notation thereon.

The views and conclusions contained herein are those of the authors and should not be interpreted as necessarily representing the official policies or endorsements, either expressed or implied, of the Air Force Research Laboratory or the U.S. Government.

actuation in general robotics [9] show that the main feature, among other interesting features, of the cable actuation is the possibility to achieve relatively high accelerations, due to the reduced mass of the most kinetically-active segments of the robots.

Since the walking robots usually have to carry an independent energy source (batteries), it is the most critical to reduce the energy consumed per distance walked. Using the cables the motors are moved to the sections of the robot that are the least kinetically-active and experience the lowest accelerations. The main benefits are: the balancing stability of the robot is improved and the energy consumption is reduced due to the reduced mass of the fast moving segments of the walking robot. It will also lead to significantly reduced overall weight of the robot. There are other benefits, too, but not directly included in the scope of this paper.

Some work has been done in the area of cable actuation in the walking robotics. A partially cable actuated hexapod is analyzed in [14].

2. KINEMATICS AND DYNAMICS ANALYSIS OF THE QUADRUPED WALKING ROBOT

2.1 The walking robot architecture

The walking robot architecture under consideration is shown in Figure 2.1. The robot architecture has 4 actuated degrees of freedom (hip, knee, ankle and the pulley) for each leg corresponding to the longitudinal motion and additional 2 degrees of freedom (hip and ankle) for each leg corresponding to the lateral motion. The actuated revolute joints of one leg are marked by “R” in Figure 2.1.

The main objective of the design was to provide a minimum DoF such that the quadruped can perform relatively “smooth” walk without frequent requests for walk direction change. Therefore, the RoboCat design considered here is the result of partial biomimicking with significant reduction in DoF. The trunk segment does not contain internal flexibility, while a biological cat has significant flexibility in the trunk, enabling the locomotion direction change. The robot architecture still enables the locomotion change through the inclusion of the two (per leg) revolute antero-posterior oriented joints at the hip and at the ankle. Other revolute joints (hip, knee, and ankle) connecting the leg segments provide the motion parallel to the sagittal (symmetry) plane.

The cables for the knee joint actuation are pulled using specially shaped pulleys situated on the trunk. This particular design detail deviates from the biological architecture and has a significant disadvantage in the fact that the cable forces can produce significant coupling between the knee and the hip joint, since the cables for the knee can generate significant torque for the hip, if not properly traced. A biological muscle for the knee does not cross the hip joint and does not generate any torque with respect to the hip.

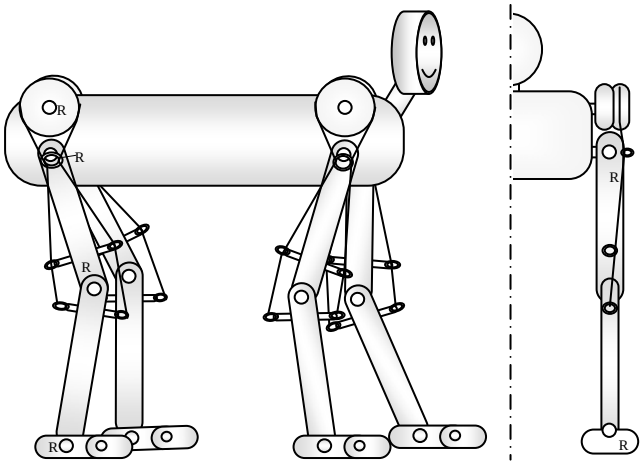

Figure 2.1 The RoboCat architecture

The length and the position of the bars with the cable attachment points about the knee joint directly influence the required (variable) cable tension over the joint motion range, as well as the (variable) cable pulling speed. Further, the required cable tension and speed (through calculation of power) are the input parameters for the motor sizing, while the transmission ratio of the motor gearbox selection directly depends on the size and the shape of the pulley.

Besides the architecture shown in Figure 2.1, several other options have been considered and/or planned to be analyzed in the future work. Considering the compactness of the architecture and the implemented hardware, it is convenient to use spherical joints rather then a combination of revolute joints for the hip. A biological hip joint is a spherical joint (3 DoF), but it is difficult to design a direct drive based actuation system for a robotic hip joint. However, using the cables, the option of using spherical joints is recommended, since it reduces the number of cables needed (4 cables for a spherical joint) comparing with separate three revolute joints (6 cables for three separate 1 DoF joints). For the sake of the simplicity, we decided to actuate only knee joint using cables.

So far, the overall architecture is presented, without specifying details. The proper sizing and the specification design detailed need to be done iteratively using a mathematical model of the system.

2.2 Mathematical modeling parameters and assumptions

The most significant assumptions for the mathematical model derivation are the following:

1) The contact surfaces between cables and the guiding holes are frictionless,
2) The cables are ideally flexible, i.e. the bending moments are zero,
3) The stretchable cables behave as linear springs,

4) The lateral motion does not produce significant inertial effects on the longitudinal motion,
5) The walk is performed on a horizontal flat plane,
6) For the sake of the dynamics analysis, the trunk can be represented as a concentrated mass at the center of gravity (CG) for the upper body,
7) The walk of the robotic system is statically stable.

The walking cycle for a leg is consisted of two main phases: the support phase and the swing phase. Since the dynamics of a stance leg with the trunk is significantly different from the dynamics of a swing leg alone, we will consider the two corresponding models of one leg dynamics with the concentrated mass of the trunk segment.

The stance leg with the concentrated mass of the trunk model is shown in Figure 2.2. The influence of the other legs to the trunk is represented through the horizontal and the vertical component of the interaction force rellocated to the trunk CG (C_t), along with the torque resulting from the reallocation of the forces.

Since the dynamics of the system is governed by several parameters of the system that are subject of the optimization through the dynamics simulation and the testing on the real hardware, we will particularly point out the sensitivity of the system behavior with respect to those quantities and analyze the way to optimize them.

Cable stiffness. One of the most important parameters is the cable spring stiffness. The physical quantity in animals that corresponds to the stiffness of the cables is the stiffness of the corresponding animal's muscles and tendons. Tendons accumulate a portion of energy that would be normally lost due to a foot-ground collision. The accumulated energy is released during the next gait cycle to decrease the amount of the kinetic energy input via the muscles. Similar effect is expected using the elastically stretchable cables for the walking robot. The contact forces are expected to smooth out as well as the joint torques, which is a desirable effect on the robot control. However, a potential problem using the stretchable cables is that the system can easily experience an oscillating behavior if there is no sufficient damping, which requires a dynamic controller to stabilize the system.

Points of the cable attachments. The positions of the points where the cables are attached relative to the joints and the geometry of the cable guidance are very important for a couple of reasons. The points where the cable guiding holes are positioned, points A' and B' in Figure 2.2, determine the torque arm with respect to the joint axis, along with the range of angular motion of the joint. Inappropriate position of the guiding holes can result in a very high cable tension required to generate a certain required torque at a specific joint angles. Therefore, optimized positions of the guiding rings and the attachment points will be determined via numerical solutions and simulations.

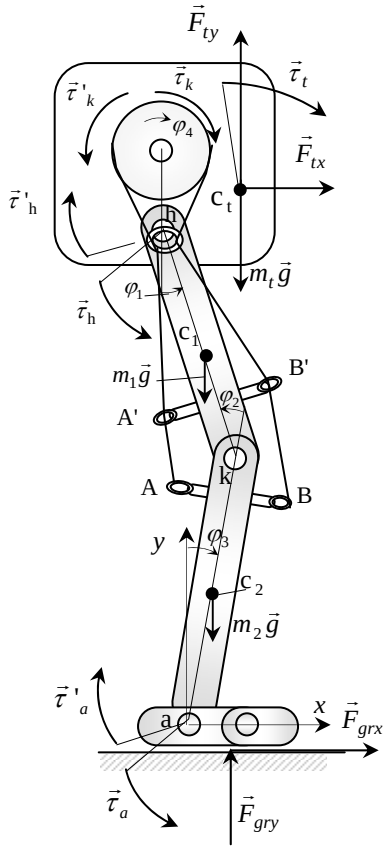

Figure 2.2 Leg-trunk model

Pulleys profile. The pulley is designed to have a variable radius profile, shown in Figure 2.3.

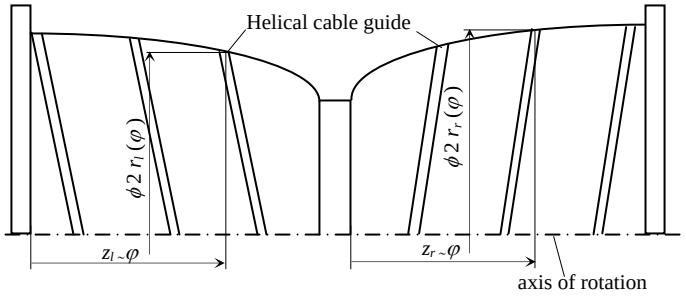

Figure 2.3 The pulley profile

The objective of the variable radius is to compensate for the difference in the cable length increase on one side and the cable length decrease on the other side of the corresponding joint, in this case the knee joint. Considering the architecture shown in Figure 2.2, the cable length increase between points B and B' is not the same as the cable length decrease between points A and A'. This causes problems if the variation of the

sum $\overline{AA'}+\overline{BB'}=f(\varphi_2)$ is significant, since a pulley with constant radius would release the same cable length as the cable length that it stores for the same angle of rotation. This difference can be compensated to a certain extent with the preloaded springs attached in series along the cables. However, the experiments showed that the spring stiffness must be significantly decreased to compensate large variation of $\overline{AA'}(\varphi_2)+\overline{BB'}(\varphi_2)$, which will reduce the effective torques it can provide to the joints. The variable radius pulley is an effective solution to enable a single motor to drive elastic cables. The design objective is that if the cable were not stretched, the pulley angle of rotation should be proportional to the rotation of the knee joint, that is

$$\frac{\varphi_4}{\varphi_2}=k=\text{constant}\,.$$

The constant *k* is a modeling parameter that has influence on the controller sensitivity and performance, and will be considered through the simulations results.

Clearly, there is no need for the variable radius pulley in the case when two motors are used to pull the two cables separately; however, the intention here is to use only one motor to drive a revolute joint.

Considering the model specifics, the mathematical model derivation requires detailed kinematic analysis, which is discussed next.

2.3 Kinematics

The objective of kinematics analysis of the robotic walker, actuated by the elastic cables, is to find the relationships between the joint angles and the positions in an inertial Cartesian coordinate system, as well as the corresponding velocities. Besides this, the kinematic analysis needs to provide the relationship between the cable speed and the angular speed of the corresponding joint. In this particular case, the aforementioned relationship represents the relationship between the pulley angular speed and the knee joint angular speed for the case when there is no change in the cable length. The cables are stretched and are assumed to behave as preloaded linear springs, deformation and kinematics are coupled with the dynamics through the deformation and forces of the springs.

Expressing the velocities of the CGs in the inertial (ground attached) Cartesian coordinate frame requires expressions of the orthogonal coordinates in terms of the joint angles, which are obtained as follows.

$$\vec{r}_{C2}=\begin{bmatrix} l_{C2}s\varphi_3 \\ l_{C2}c\varphi_3 \end{bmatrix},\ \vec{r}_{C1}=\begin{bmatrix} l_2s\varphi_3-l_{C1}s\varphi_{23} \\ l_2c\varphi_3+l_{C1}c\varphi_{23} \end{bmatrix},\qquad (2.1)$$

$$\vec{r}_T=\begin{bmatrix} l_2s\varphi_3-l_1s\varphi_{23}+l_{p1}s\varphi_{123}+l_{p2}c\varphi_{123} \\ l_2c\varphi_3+l_1c\varphi_{23}+l_{p1}c\varphi_{123}-l_{p2}s\varphi_{123} \end{bmatrix},$$

where l_{Ci}, $(i=1,2)$ are the lower parts of the leg segments lengths from the joints to the CGs, l_{p1} and l_{p2} are the *y* and *x* coordinates of the trunk CG with respect to the hip joint, φ_i, $(i=1,2,3,4)$ are the joint angles denoted in Figure 2.2, φ_{ij} and φ_{ijk}, $(i,j,k=1,2,3)$ are the combined angles as $\varphi_{ij}=\varphi_i-\varphi_j$ and $\varphi_{ijk}=\varphi_i-\varphi_j+\varphi_k$, and abbreviation for sine and cosine functions is used as $\mathrm{s}\psi=\sin\psi$, $\mathrm{c}\psi=\cos\psi$, with ψ denoting any of the aforementioned (combined) angles.

By differentiating (2.1) we obtain the velocities

$$\vec{v}_{C2}=l_{C2}\dot{\varphi}_3\begin{bmatrix} c\varphi_3 \\ -s\varphi_3 \end{bmatrix},\ \vec{v}_{C1}=\begin{bmatrix} l_2c\varphi_3\dot{\varphi}_3-l_{C1}c\varphi_{23}\dot{\varphi}_{23} \\ -l_2s\varphi_3\dot{\varphi}_3-l_{C1}s\varphi_{23}\dot{\varphi}_{23} \end{bmatrix},$$
$$\vec{v}_T=\begin{bmatrix} l_2c\varphi_3\dot{\varphi}_3-l_1c\varphi_{23}\dot{\varphi}_{23}+l_{p1}c\varphi_{123}\dot{\varphi}_{123}-l_{p2}s\varphi_{123}\dot{\varphi}_{123} \\ -l_2s\varphi_3\dot{\varphi}_3-l_1s\varphi_{23}\dot{\varphi}_{23}-l_{p1}s\varphi_{123}\dot{\varphi}_{123}-l_{p2}c\varphi_{123}\dot{\varphi}_{123} \end{bmatrix}.\qquad (2.2)$$

Besides the relationships (2.1) and (2.2), we need an appropriate function that indicates how much and with which rate the cable should be pulled to obtain a desired joint angle and an angular speed. The cable length change on the two sides of the pulley in Figure 2.2 is due to the change in the joint angle and due to the change in the cable tension. The cable length change rate due to the change in the knee angle φ_2 is

$$\frac{\partial}{\partial\varphi_2}l_r(\varphi_2,S_r)\dot{\varphi}_2=\frac{d}{d\varphi_2}\overline{BB}(\varphi_2)\dot{\varphi}_2=\frac{h_{BBs}c\varphi_2-h_{BBc}s\varphi_2}{\overline{BB}(\varphi_2)}\dot{\varphi}_2\,,$$
$$\frac{\partial}{\partial\varphi_2}l_l(\varphi_2,S_l)\dot{\varphi}_2=\frac{d}{d\varphi_2}\overline{AA}(\varphi_2)\dot{\varphi}_2=\frac{-h_{AAs}c\varphi_2-h_{AAc}s\varphi_2}{\overline{AA}(\varphi_2)}\dot{\varphi}_2,\qquad (2.3)$$

where l_r and l_l are the cable lengths on the right and on the left of the pulley, respectively, S_r and S_l are corresponding cable tensions, and

$$h_{BBs}=h_{1r}h_3+h_2h_{4r}\,,\quad h_{BBc}=-h_2h_3+h_{1r}h_{4r}\,,$$
$$h_{AAs}=h_{1l}h_3+h_2h_{4l}\,,\quad h_{AAc}=-h_2h_3+h_{1l}h_{4l}\,,$$

with h_{1r}, h_{1l}, h_2, h_3, h_{4r}, h_{4l} denoting the position of the cables attachment points relatively to the knee joint, as shown in Figure 2.4.

The total cable length changes on the two sides of the pulley are

$$\Delta l_r(\varphi_2,S_r)=(S_r-S_{r0})\frac{1}{k_{sr}}+\overline{BB'}(\varphi_2)-\overline{BB'}(0)\,,$$

$$\Delta l_l(\varphi_2, S_l) = (S_l - S_{l0})\frac{1}{k_{sl}} + \overline{AA'}(\varphi_2) - \overline{AA'}(0), \quad (2.4)$$

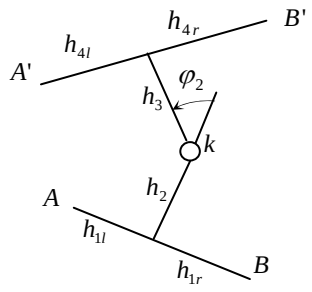

Figure 2.4 The cable attachment points parameters

where k_{sr}, k_{sl} are the cable spring stiffness coefficients for the right and left cable segments, respectively.

Now, we need to determine the pulley profile function that will provide proportional rotations of the knee joint and the pulley, for an approximately constant cable tension. The general profile of the pulley is shown in Figure 2.3, which indicates two rigidly joined segments corresponding to the right and left cable. The objective of this design is to reduce normally large spring's deformations due to the joint angles changes (geometrical changes).

To compensate the necessary difference in the cable stored on and released from the pulley, the radius functions $r_r(\varphi_4)$ and $r_l(\varphi_4)$ must cancel nonlinearity in $\overline{AA'}(\varphi_2)$ and $\overline{BB'}(\varphi_2)$. In this way, the two functions are

$$r_s(\varphi_4) = \begin{cases} R_{\min}, & \text{for } \pm\left.\dfrac{d\overline{PP'}(\varphi_2)}{d\varphi_2}\right|_{\varphi_2=k\varphi_4}\left(\dfrac{\delta\varphi_2}{\delta\varphi_4}\right)_{\text{des}} < R_{\min} \\ R_{\max}, & \text{for } \pm\left.\dfrac{d\overline{PP'}(\varphi_2)}{d\varphi_2}\right|_{\varphi_2=k\varphi_4}\left(\dfrac{\delta\varphi_2}{\delta\varphi_4}\right)_{\text{des}} > R_{\max}, \\ \pm\left.\dfrac{d\overline{PP'}(\varphi_2)}{d\varphi_2}\right|_{\varphi_2=k\varphi_4}\left(\dfrac{\delta\varphi_2}{\delta\varphi_4}\right)_{\text{des}}, & \text{otherwise.} \end{cases} \quad (2.6)$$

where $\left(\dfrac{\delta\varphi_2}{\delta\varphi_4}\right)_{\text{des}} = k$ is the desired ratio of the two rotations, $R_{\min}$ is the minimum (positive) radius of the pulley and the derivatives are given in (2.3), the plus sign is for "s=r" and "$P = B$". The ratio cannot be precisely constant due to the fact that the cable is stretchable and we cannot compensate the general cable tension force, since it is not only a function of the angles, but also depends on the inertial forces and the payload.

For the following parameters: $h_{1r} = h_{1l} = h_2 = h_3 = 0.1$ m, $h_{4r} = h_{4l} = 0.1$m, k=0.5, the radii functions of the two pulley segments are:

$$r_s(\varphi_4) = \begin{cases} R_{\min}, & \text{for } 0.05\dfrac{\cos(0.5\varphi_4)}{\sqrt{1\pm\sin(0.5\varphi_4)}} < R_{\min} \\ R_{\max}, & \text{for } 0.05\dfrac{\cos(0.5\varphi_4)}{\sqrt{1\pm\sin(0.5\varphi_4)}} > R_{\max} \\ 0.05\dfrac{\cos(0.5\varphi_4)}{\sqrt{1\pm\sin(0.5\varphi_4)}}, & \text{otherwise.} \end{cases}$$

(in meters), where plus sign is for "s=r".

The profile plot for the set of the parameters is shown in Figure 2.5.

The pulley profile shown in Figure 2.5 is consisted of the two sections corresponding to the back and the front cable of the knee drive unit. The derivation of the pulley assumes that the knee joint design restricts hyperextensions, which means that the angle φ_2 takes only positive values for the back legs and only negative values for the front legs of the RoboCat. We can see that two radii have the same value only for $\varphi_2 = 0$, when the symmetry exists.

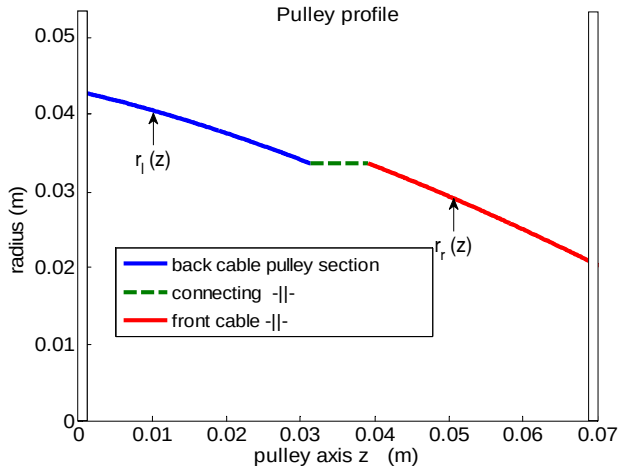

Figure 2.5 The pulley profile

Finally, depending on the method that is used for the dynamics model derivation, we would need the acceleration vector expressions for the centers of gravity of the major architectural parts (links, motors, battery). However, the method that we will use requires the expressions for the velocity of the centers of gravity. Now, we will use the kinematics expressions to derive the dynamics model of the robot.

2.4 Dynamics of the RoboCat

Using the Lagrange energy method, a set of nonlinear differential equations of second order is derived. Since the derivation details would take significant space, we will include the final results for every particular DOF.

The dynamics of the system can be represented by the matrix equation

$$\left[\mathrm{M}(\vec{\varphi}(t))\right]\ddot{\vec{\varphi}}(t)+\left[\mathrm{C}(\vec{\varphi}(t),\dot{\vec{\varphi}}(t))\right]\dot{\vec{\varphi}}(t)+\left[\mathrm{P}(\vec{\varphi}(t))\right]=\vec{\tau}(t)\,, \quad (2.7)$$

where $\vec{\varphi}(t)$, $\dot{\vec{\varphi}}(t)$ and $\ddot{\vec{\varphi}}(t)$ are the joint angle, velocity and acceleration vectors, respectively, $\left[\mathrm{M}(\vec{\varphi}(t))\right]$ is the inertial properties matrix; $\left[\mathrm{C}(\vec{\varphi}(t),\dot{\vec{\varphi}}(t))\right]$ is the angular speed coupling matrix, $\left[\mathrm{P}(\vec{\varphi}(t))\right]$ is the vector that includes the gravity terms and cable tension terms and $\vec{\tau}(t)$ is the vector of torques acting at the joints. The product $\left[\mathrm{C}(\vec{\varphi}(t),\dot{\vec{\varphi}}(t))\right]\dot{\vec{\varphi}}(t)$ represents all combined products of the joints angular speed, which is consisted of the Coriolis and relative normal accelerations. For the sake of conciseness, the matrices $\left[\mathrm{M}(\vec{\varphi})\right]$ and $\left[\mathrm{C}(\vec{\varphi}(t),\dot{\vec{\varphi}}(t))\right]$ are given by the columns in the **Appendix**.

The vector of the conservative generalized forces $\left[\mathrm{P}(\vec{\varphi}(t))\right]$ requires an explanation that is related to the further analysis, and we present it below.

The vector of the conservative generalized forces $\left[P(\vec{\varphi})\right]$ is

$$\left[\mathrm{P}\right]=$$

$$\begin{bmatrix} m_{\mathrm{T}}\,g\,(-l_{\mathrm{p1}}s\varphi_{123}-l_{\mathrm{p2}}c\varphi_{123}) \\ \hline -m_1\,g\,l_{\mathrm{C1}}s\varphi_{23}-m_{\mathrm{T}}\,g\,(l_1s\varphi_{23}-l_{\mathrm{p1}}s\varphi_{123}-l_{\mathrm{p2}}c\varphi_{123})+ \\ k_{\mathrm{Sr}}\Delta l_R\dfrac{h_{\mathrm{BBs}}c\varphi_2-h_{\mathrm{BBc}}s\varphi_2}{\overline{BB'}(\varphi_2)}+k_{\mathrm{Sl}}\Delta l_L\dfrac{-h_{\mathrm{AAs}}c\varphi_2-h_{\mathrm{AAc}}s\varphi_2}{\overline{AA'}(\varphi_2)} \\ \hline -m_2\,g\,l_{\mathrm{C2}}s\varphi_3-m_1\,g\,(l_2s\varphi_3-l_{\mathrm{C1}}s\varphi_{23})+ \\ m_{\mathrm{T}}\,g\,(-l_2s\varphi_3+l_1s\varphi_{23}-l_{\mathrm{p1}}s\varphi_{123}-l_{\mathrm{p2}}c\varphi_{123}) \end{bmatrix}, \quad (2.8)$$

where k_{Sr}, k_{Sl} are the cable stiffness coefficients for the front and the back cable, respectively, and

$$\Delta l_R=\Delta l_R(\varphi_2,\varphi_4)=\overline{BB'}(\varphi_2)-\overline{BB'}_0+\frac{S_{R0}}{k_{Sr}}-\int_0^{\varphi_4}R_{PR}(\theta)\,d\theta\,, \quad (2.9)$$

$$\Delta l_L=\Delta l_L(\varphi_2,\varphi_4)=\overline{AA'}(\varphi_2)-\overline{AA'}_0+\frac{S_{L0}}{k_{Sl}}+\int_0^{\varphi_4}R_{PL}(\theta)\,d\theta\,,$$

are the deformation of cable springs. The new quantities included in (2.9) denote the following: S_{R0} and S_{L0} are the cables pre-tensions, $R_{PR}(\theta)$ and $R_{PL}(\theta)$ are the two pulley variable radii given by (2.6) and θ is the geometrical angle of the cable guide on the pulley, shown in Figure 2.3. The integrals in (2.9) represent the stored cable along the pulley thread.

The vector of the torques $\vec{\tau}$ in (2.7) is

$$\vec{\tau}(t)=\left[\tau_{\mathrm{h}}(t)\quad 0\quad \tau_{\mathrm{a}}(t)\right]^{\mathrm{T}}, \quad (2.10)$$

where $\tau_{\mathrm{h}}(t)$ and $\tau_{\mathrm{a}}(t)$ are the torques at the hip and the ankle joints, respectively. The torque at the knee joint is considered through the cable tension expressions in the vector $\left[P(\vec{\varphi})\right]$.

If we consider the system shown in Figure 2.1 precisely, we would have 4 DOF and, consequently, matrices in (2.7) would have the size 4 by 4 and the vectors would be 4 by 1, which would increase the computational efforts in the system controller algorithm. By neglecting the moment of inertia of the pulley drive system, the mathematical model is reduced to three differential equations of the second order. However, we need the moment balancing equation of the pulley – cables system. The equation is

$$-k_{\mathrm{Sr}}\Delta l_R(\varphi_2,\varphi_4)R_{PR}(\varphi_4)+k_{\mathrm{Sl}}\Delta l_L(\varphi_2,\varphi_4)R_{PL}(\varphi_4)=\tau_{\mathrm{k}}(t)\,, \quad (2.11)$$

where $\tau_{\mathrm{k}}(t)$ is the torque provided by the pulley drive.

The equations (2.7) through (2.11), along with the kinematic relations, and the matrices $\left[\mathrm{M}(\vec{\varphi})\right]$ and $\left[\mathrm{C}(\vec{\varphi}(t),\dot{\vec{\varphi}}(t))\right]$ shown in **Appendix** represent the mathematical model of the walking robot. For the purpose of the controller design, the mathematical model of the form (2.7) needs to be converted into a state space model, which is, a set of the first order differential equations.

2.5 State space model

Since the mass matrix in (2.7) is invertible, the equation can be explicitly solved with respect to the angular accelerations as

$$\ddot{\vec{\varphi}}=-\left[M(\vec{\varphi})\right]^{-1}\left[C(\vec{\varphi},\dot{\vec{\varphi}})\right]\dot{\vec{\varphi}}-\left[M(\vec{\varphi})\right]^{-1}\left[P(\vec{\varphi})\right]+\left[M(\vec{\varphi})\right]^{-1}\vec{\tau}\,, \text{ or}$$

$$\ddot{\vec{\varphi}}=\vec{f}(\vec{\varphi},\dot{\vec{\varphi}})+G(\vec{\varphi})\,\vec{\tau}\,, \quad (2.12)$$

where

$$\vec{f}(\vec{\varphi},\dot{\vec{\varphi}})=-\left[M(\vec{\varphi})\right]^{-1}\left[C(\vec{\varphi},\dot{\vec{\varphi}})\right]\dot{\vec{\varphi}}-\left[M(\vec{\varphi})\right]^{-1}\left[P(\vec{\varphi})\right], \text{ and}$$

$$G(\vec{\varphi})=\left[M(\vec{\varphi})\right]^{-1}.$$

By assigning variables: $\xi_1 = \varphi_1$, $\xi_2 = \dot{\xi}_1 = \dot{\varphi}_1$, $\xi_3 = \varphi_2$, $\xi_4 = \dot{\xi}_3 = \dot{\varphi}_2$, $\xi_5 = \varphi_3$, and $\xi_6 = \dot{\xi}_5 = \dot{\varphi}_3$, the state space model has the form

$$\begin{bmatrix} \dot{\xi}_1 \\ \dot{\xi}_2 \\ \dot{\xi}_3 \\ \dot{\xi}_4 \\ \dot{\xi}_5 \\ \dot{\xi}_6 \end{bmatrix} = \begin{bmatrix} \xi_2 \\ f_2(\vec{\xi}) \\ \xi_4 \\ f_4(\vec{\xi}) \\ \xi_6 \\ f_6(\vec{\xi}) \end{bmatrix} + \begin{bmatrix} 0 & 0 & 0 \\ G_{21}(\vec{\xi}) & G_{22}(\vec{\xi}) & G_{23}(\vec{\xi}) \\ 0 & 0 & 0 \\ G_{41}(\vec{\xi}) & G_{42}(\vec{\xi}) & G_{43}(\vec{\xi}) \\ 0 & 0 & 0 \\ G_{61}(\vec{\xi}) & G_{62}(\vec{\xi}) & G_{63}(\vec{\xi}) \end{bmatrix} \begin{bmatrix} \tau_{\mathrm{h}} \\ \tau_{\mathrm{k}} \\ \tau_{\mathrm{a}} \end{bmatrix}, \qquad (2.13)$$

where $f_i(\vec{\xi})$, $G_{ij}(\vec{\xi})$ (i=2,4,6; j=1,2,3) represents the entries of the functions in (2.12).

2. 6 Interconnections with other supporting legs

The interconnections with other supporting legs can be viewed as disturbances in case when it is not convenient to expand the mathematical model of the system and the controller complexity. However, if it is necessary to obtain better performance of the controller, the interconnections can be modeled as follows.

The interconnections between the supporting leg models can be interpreted through the interconnecting force and torque, as shown in Figure 2.2. The interconnecting forces and torque can be included in the existing model through the joint torques. The augmented torque vector given by (2.10) becomes

$$\begin{aligned} \tau_1' &= \tau_{\mathrm{h}} + \tau_t + F_{tx}(l_{P1}c\varphi_{123} - l_{P2}s\varphi_{123}) + F_{ty}(-l_{P1}s\varphi_{123} - l_{P2}c\varphi_{123}), \\ \tau_2' &= -\tau_t + F_{tx}(-l_1c\varphi_{23} - l_{P1}c\varphi_{123} + l_{P2}s\varphi_{123}) + \\ &\quad F_{ty}(-l_1c\varphi_{23} - l_{P1}s\varphi_{123} + l_{P2}c\varphi_{123}), \qquad (2.14) \\ \tau_3' &= \tau_{\mathrm{a}} + \tau_t + F_{tx}(l_2c\varphi_3 + l_1c\varphi_{23} + l_{P1}c\varphi_{123} - l_{P2}s\varphi_{123}) + \\ &\quad F_{ty}(-l_2s\varphi_3 + l_1s\varphi_{23} - l_{P1}s\varphi_{123} - l_{P2}c\varphi_{123}), \end{aligned}$$

where the meaning of the interconnecting forces and the torque is explained earlier and shown in Figure 2.2. The next section will show how the model is used to design a controller.

3. CONTROLLER DESIGN

The controller design for the robotic walker will be based on the trajectory regulation control [10].

3.1 Controller architecture

The control system architecture, shown in Figure 3.1, is consisted of [10, 11]:

(a) Nominal trajectories generator,
(b) Inverse dynamics for nominal control calculation
(c) Tracking error regulation controller,
(d) Measurement system, and
(e) Plant

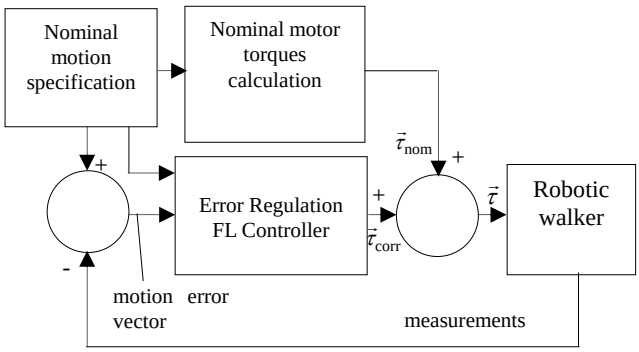

Figure 3.1 The trajectory regulation controller architecture

The nominal motion specification block generates the joint trajectories that will provide a balanced walk. The information about the nominal joint angles at every time-step is sent to the error dynamics controller and the nominal torques generator. The nominal torques are generated based on the inverse dynamics mathematical model. Since the mathematical model of the robot is not an exact description of the dynamic behavior, there will be errors in the resulting motion. The amount of the resulting motion deviation from the desired motion is calculated based on the measurements of the joint's angles which is used by the error dynamics controller to generate the correction torques.

The inverse dynamics that is used to generate the nominal torques is obtained directly from (2.7), where the torques are explicitly expressed in terms of the functions of angles and their first two derivatives. However, the derivatives of the input signals must be obtained via pseudo-differentiators of the form (in the Laplace domain)

$$\Phi(s) = \frac{s}{\varepsilon s + 1}, \quad \varepsilon \in \left[10^{-3}, 10^{-2}\right],$$

to obtain physically realizable derivatives. Since the controller architecture is based on the error dynamics, we need to obtain the appropriate error dynamics model.

3.2 Error dynamics

The error dynamics model is based on the state space model (2.14) and it has the following form

$$\begin{bmatrix} \dot{\tilde{\xi}}_1 \\ \dot{\tilde{\xi}}_2 \\ \dot{\tilde{\xi}}_3 \\ \dot{\tilde{\xi}}_4 \\ \dot{\tilde{\xi}}_5 \\ \dot{\tilde{\xi}}_6 \end{bmatrix} = \begin{bmatrix} \tilde{\xi}_2 \\ f_2(\vec{\xi}) - f_2(\vec{\bar{\xi}}) \\ \tilde{\xi}_4 \\ f_4(\vec{\xi}) - f_4(\vec{\bar{\xi}}) \\ \tilde{\xi}_6 \\ f_6(\vec{\xi}) - f_6(\vec{\bar{\xi}}) \end{bmatrix} + \begin{bmatrix} 0 & 0 & 0 \\ G_{21}(\vec{\bar{\xi}}) & G_{22}(\vec{\bar{\xi}}) & G_{23}(\vec{\bar{\xi}}) \\ 0 & 0 & 0 \\ G_{41}(\vec{\bar{\xi}}) & G_{42}(\vec{\bar{\xi}}) & G_{43}(\vec{\bar{\xi}}) \\ 0 & 0 & 0 \\ G_{61}(\vec{\bar{\xi}}) & G_{62}(\vec{\bar{\xi}}) & G_{63}(\vec{\bar{\xi}}) \end{bmatrix} \begin{bmatrix} \tilde{\tau}_{\mathrm{h}} \\ \tilde{\tau}_{\mathrm{k}} \\ \tilde{\tau}_{\mathrm{a}} \end{bmatrix}, \tag{3.1}$$

where $\tilde{\xi}_i = \xi_i - \bar{\xi}_i$ and $\bar{\xi}_i$ (i=1,…,6) are, respectively, the error and the nominal value of the i-th component of the state vector, and $\tilde{\tau}_{\mathrm{h}}$, $\tilde{\tau}_{\mathrm{k}}$, $\tilde{\tau}_{\mathrm{a}}$ are the corrective torque values, generated by the feedback controller with the objective to satisfy $\left\| \vec{\tilde{\xi}} \right\| \to 0$ (exponentially). The way the error vector is stabilized is discussed in the following section.

3.3 Control law

The control law should provide the corrective torques such that the errors converge to zero with an exponential decay. To achieve this goal, the control inputs cancel the nonlinearity (FL technique) and introduce the terms proportional to the errors of the states as follows.

$$\begin{aligned} G_{21}(\vec{\bar{\xi}})\tilde{\tau}_{\mathrm{h}} + G_{22}(\vec{\bar{\xi}})\tilde{\tau}_{\mathrm{k}} + G_{23}(\vec{\bar{\xi}})\tilde{\tau}_{\mathrm{a}} &= \tilde{b}_{g1}, \\ G_{41}(\vec{\bar{\xi}})\tilde{\tau}_{\mathrm{h}} + G_{42}(\vec{\bar{\xi}})\tilde{\tau}_{\mathrm{k}} + G_{43}(\vec{\bar{\xi}})\tilde{\tau}_{\mathrm{a}} &= \tilde{b}_{g2}, \\ G_{61}(\vec{\bar{\xi}})\tilde{\tau}_{\mathrm{h}} + G_{62}(\vec{\bar{\xi}})\tilde{\tau}_{\mathrm{k}} + G_{63}(\vec{\bar{\xi}})\tilde{\tau}_{\mathrm{a}} &= \tilde{b}_{g3}, \end{aligned} \tag{3.2}$$

where

$$\begin{aligned} \tilde{b}_{g1} &= -f_2(\vec{\xi}) + f_2(\vec{\bar{\xi}}) - k_{21}\tilde{\xi}_1 - k_{22}\tilde{\xi}_2, \\ \tilde{b}_{g2} &= -f_4(\vec{\xi}) + f_4(\vec{\bar{\xi}}) - k_{43}\tilde{\xi}_3 - k_{44}\tilde{\xi}_4, \\ \tilde{b}_{g3} &= -f_6(\vec{\xi}) + f_6(\vec{\bar{\xi}}) - k_{65}\tilde{\xi}_5 - k_{66}\tilde{\xi}_6, \end{aligned}$$

and k_{ij} (i=2,4,6; j=i-1, i) are the constants that need to be determined, such that the closed control loop error dynamics are exponentially stable and have desired transient behavior.

Particularly, we can set up the constraint that the system has less than 5% overshoot, and the settling time less than 0.5 seconds for each joint rotational DOF, which results in the damping coefficient $\zeta > 0.69$ and the natural frequency $\omega_{\mathrm{n}} > 11.59 \frac{\mathrm{rad}}{\mathrm{s}}$. To obtain the two values, the coefficients k_{ij} need to have the following values

$$k_{21} = k_{41} = k_{61} = 134.3 \left(\frac{\mathrm{rad}}{\mathrm{s}}\right)^2, \; k_{22} = k_{44} = k_{66} = 16 \left(\frac{\mathrm{rad}}{\mathrm{s}}\right).$$

Finally, the control law is

$$\vec{\tilde{\tau}} = G_r^{-1}\vec{\tilde{b}}_g, \tag{3.3}$$

where G_r is the reduced input matrix evaluated at the nominal trajectory $\vec{\bar{\xi}}$. Next, we will evaluate the performance of the control law via simulation results.

3.4 Simulation results and the performance analysis

The block diagram, shown in Figure 3.1, is implemented in the Matlab/Simulink; the control law is tested on a combination of ramp inputs for the joints angles and the simulation results are shown in the following figures.

The nominal joint angles and the smooth pseudo-differentiator obtained angular velocity trajectories are shown in Figure 3.2.

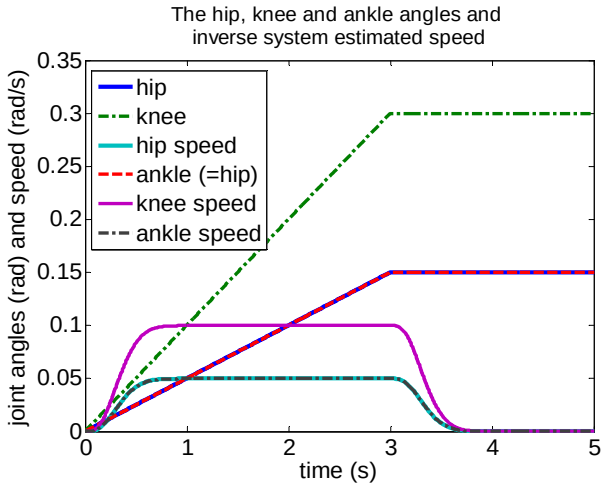

Figure 3.2 Nominal trajectories

The nominal torques predicted by the inverse dynamics block are shown in Figure 3.3.

The results in the nominal torques plot agree with the expected results since force arm is significantly greater for the knee joint than for the other two joints. The hip joint has low predicted torque due to the fact that the CG of the trunk for the prescribed motion is considered vertically above the hip.

Cable tensions needed to provide the knee joint angular trajectory are shown in Figure 3.4. The plot shows that the cables pre-tension was 50 N and could have been even reduced and still avoid slack cable.

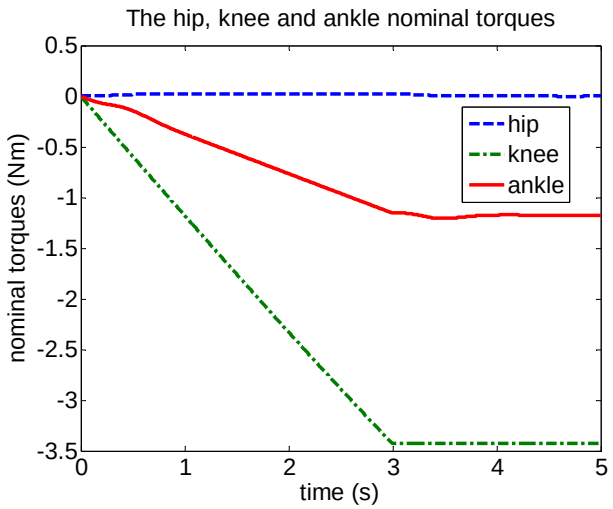

Figure 3.3 Nominal joint torques

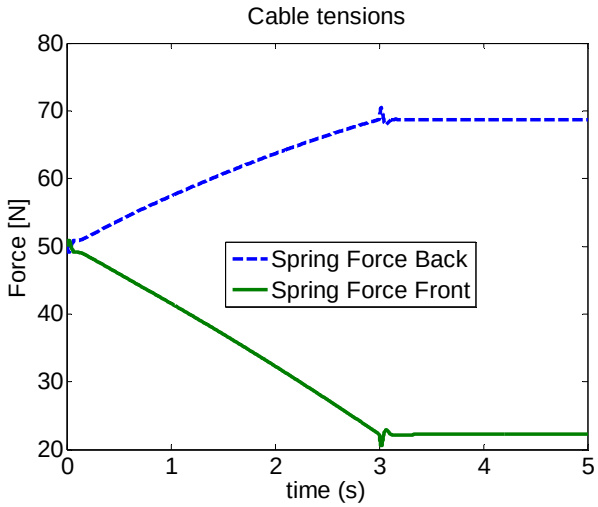

Figure 3.4 The cable tensions

The comparison between the actual angles versus the desired angles is shown in Figure 3.5. The plot shows very low errors of the actual trajectories (the ankle and the hip have the same nominal trajectory in the plot). Deviation is noticeable at the instants when there are sharp changes in the desired trajectory slope.

The deviation of the actual angles from the desired angles can be seen in the errors plot shown in Figure 3.6.

Total torques supplied to the joints of the robot model are shown in Figure 3.7. If the nominal torques, shown in Figure 3.3, are compared with the total torques, significant corrective values of the torques can be noticed at the instants when there is significant change in the desired speed of the joints, due to the inertial effects and the effect of the pseudo-differentiation, as well.

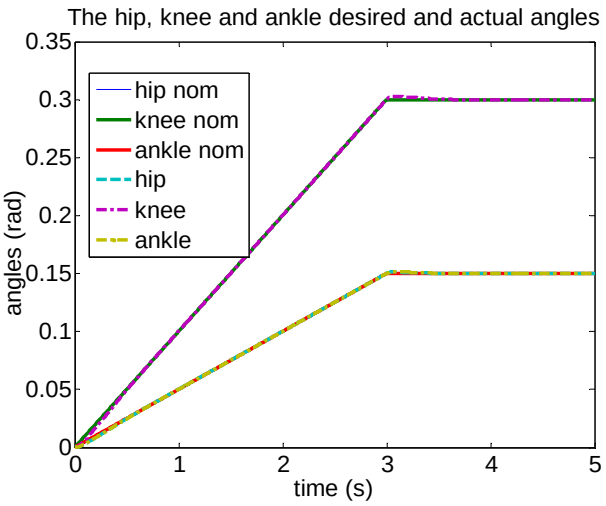

Figure 3.5 The actual versus desired trajectories

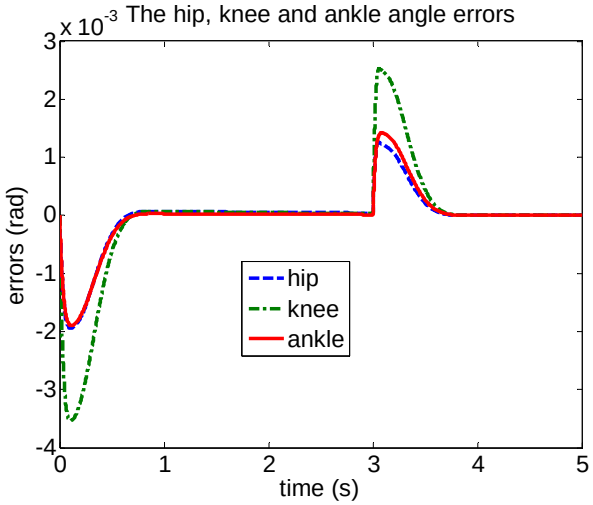

Figure 3.6 The hip, knee and ankle joint angle errors

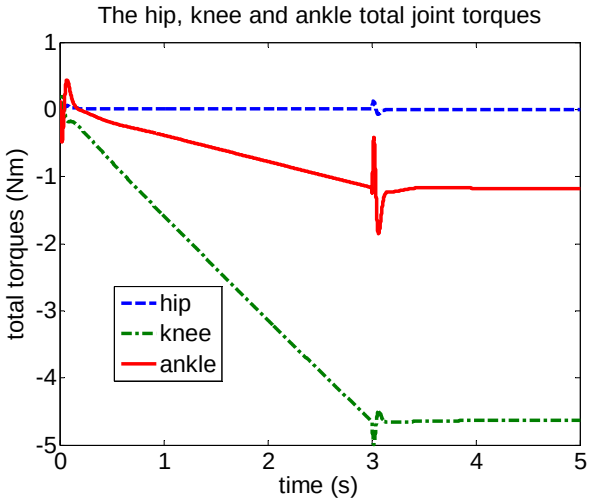

Figure 3.7 Total joint torques

4. CONCLUSION AND FUTURE WORK

The paper presented a novel actuation system of a robotic walker. The actuation system is based on a combination of the direct drive actuation and a novelty in walking robotics, the stretchable cable actuation. Several benefits are introduced using the cables to actuate joints. The energy consumption is reduced through the reduction of the inertial forces on the most motion active parts of the robot. The need of using two different pulley-motor pairs to actuate a revolute joint in case of using non-stretchable cables is compensated using the stretchable cables with the design of the special pulley profile. The threaded pulley profile with the variable radius ensured that, along with relatively small deformations of the cable spring, the cables do not become loose, which would lead directly into complications with "pure transport delays" in the control law.

The mathematical model is derived, with respect to the assumptions that are listed. The leg-trunk dynamics model is presented in state space form and the corresponding error dynamics is used to design the controller using the trajectory regulation control with an open-loop nominal controller and a closed loop tracking error regulation controller. The nominal controller is based on the inverse dynamics model of the plant. The closed-loop controller is based on the feedback linearization control, where plant nonlinearity is cancelled by state feedback, and desired linear dynamics are assigned.

It is shown how the model can be combined through the interconnection quantities with another leg-trunk model to consider the impact from the other supporting legs.

The performance of the joint trajectories tracking was analyzed using simulations, which showed satisfactory results of tracking the prescribed joint trajectories. The possible problematic cases of the tracking would be the cases with the sharp changes and/or associated noise in the desired trajectories, due to the need of finding (approximate) derivatives.

Planned future work is to implement the robot control algorithm in a real hardware. Certain steps in this direction have already been made on a quadruped robot – RoboCat, however using an open loop control algorithm that produced certain oscillation in the joints motion. It is expected that the implementation of the presented algorithm will result in a better performance, besides the inherent beneficial features of using the (stretchable) cables for the robot actuation, which were described in the paper.

Currently the RoboCat employs a statically stable walking gait, with standard Radio Controlled (R/C) servo motors as actuators, as shown in Figure 4.1.

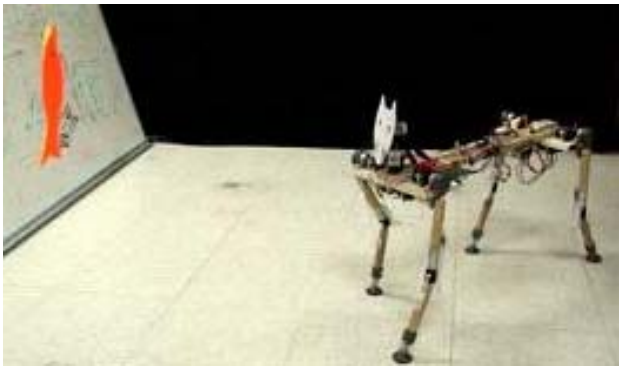

Figure 4.1 The RoboCat (see the video clip link below)

The shoulder/hip joints have one DOF direct actuation, and the knee/elbow joints have one DOF elastic cable driven actuation. The servo motors have built-in angular position controllers, which restricted the motion control to be a sequence of position commands to the joints. Such joint motion control scheme is open-loop in nature, and the performance is very limited, which can be seen at

http://www.youtube.com/watch?v=sZZpKn_nDIc
http://www.youtube.com/watch?v=ZCydQB9Vyfo

We will implement the closed-loop motion control scheme developed in this paper in the future, which should improve the performance significantly.

Due to a limitation on the number of pages, we have not included another important segment of analysis, the swing leg dynamics and control. This will be included in a future paper.

ACKNOWLEDGMENT

We thank Mr. Justin Mamrak, a PhD student at Electrical Engineering and Computer Science Department at Ohio University, for participating in assembling the hardware.

REFERENCES

[1] Giovanni A. Cavagna, Norman C. Heglund, and C. Richard Taylor, Mechanical work in terrestrial locomotion: two basic mechanisms for minimizing energy expenditure. *Am J Physiol.*; **233,** 1977.

[2] Brian R. Umberger and Philip E. Martin, "Mechanical power and efficiency of level walking with different stride rates", *The Journal of Experimental Biology*, **210**, pp. 3255-326, 2007.

[3] Ruina, A., Bertram, J. E., & Srinivasan, M., A collisional model of the energetic cost of support work qualitatively explains leg sequencing in walking and galloping, pseudo-elastic leg behavior in running and the walk-to-run transition. *Journal of Theoretical Biology*, **237**, pp. 170–192, 2005.

[4] Vanderborght Bram, Van Ham Ronald, Verrelst Bjorn, Van Damme Michael, Lefeber Dirk, "Overview of the Lucy Project: Dynamic Stabilization of a Biped Powered by

Pneumatic Artificial Muscles," *Advanced Robotics*, **22**, pp. 1027–1051, 2008.
[5] http://www.humanoid.waseda.ac.jp/booklet/kato_4.html
[6] Ali E. Aliev et al., "Giant-Stroke, Superelastic Carbon Nanotube Aerogel Muscles," *Science*, **323**, pp. 1575-1578, 2009.
[7] Ray H. Baughman, "Playing Nature's Game with Artificial Muscles," *Science*, **308**, pp. 63-65, 2005.
[8] Yoseph Bar-Cohen and Sean Leary, "Electroactive Polymers as Artificial Muscles changing Robotics Paradigms," National Space and Missile Materials Symposium, 2000.
[9] E. Kljuno and R.L. Williams II, "Vehicle Simulation System: Controls and Virtual-Reality-Based Dynamics Simulation", *Journal of Intelligent and Robotic Systems*, **52**, pp. 79-99, 2008.
[10] Khalil, H. K., "Nonlinear Systems," 2nd Edition, Englewood Cliffs, NJ, Prentice-Hall, 1996.
[11] Jim J. Zhu, "Lecture Notes on Nonlinear Systems Control: Blue Book," Ohio University, 2008.
[12] http://world.honda.com/ASIMO/
[13] http://www.takanishi.mech.waseda.ac.jp/top/research/wabian/index.htm
[14] Alan P. Bowling, "Mass Distribution Effects on Dynamic Performance of a Cable-Driven Hexapod," ASME Journal of Mechanical Design, vol. 129, no. 8, pp. 887-890, 2007.

APPENDIX
THE INERTIAL PROPERTIES AND THE COUPLING MATRICES

The inertia properties matrix $\left[\mathrm{M}(\vec{\varphi}(t))\right]$ is given by the following columns.

$\left[\mathrm{M}(:,1)\right]=$

$$\begin{bmatrix} m_{\mathrm{T}}(l_{\mathrm{p1}}^2+l_{\mathrm{p2}}^2)+I_{\mathrm{T}} \\ m_{\mathrm{T}}(l_1(-l_{\mathrm{p1}}c\varphi_1+l_{\mathrm{p2}}s\varphi_1)-(l_{\mathrm{p1}}^2+l_{\mathrm{p2}}^2))-I_{\mathrm{T}} \\ m_{\mathrm{T}}(l_{\mathrm{p1}}^2+l_{\mathrm{p2}}^2+l_2(l_{\mathrm{p1}}c\varphi_{12}-l_{\mathrm{p2}}s\varphi_{12})+l_1(l_{\mathrm{p1}}c\varphi_1-l_{\mathrm{p2}}s\varphi_1))+I_{\mathrm{T}} \end{bmatrix},$$

$\left[\mathrm{M}(:,2)\right]=$

$$\begin{bmatrix} m_{\mathrm{T}}(l_1(-l_{\mathrm{p1}}c\varphi_1+l_{\mathrm{p2}}s\varphi_1)-(l_{\mathrm{p1}}^2+l_{\mathrm{p2}}^2))-I_{\mathrm{T}} \\ \hline m_1l_{\mathrm{C1}}^2+m_{\mathrm{T}}(l_{\mathrm{p1}}^2+l_{\mathrm{p2}}^2-l_1^2+2l_1(l_{\mathrm{p1}}c\varphi_1-l_{\mathrm{p2}}s\varphi_1))+I_{\mathrm{T}}+I_1 \\ \hline -m_1(l_{\mathrm{C1}}^2+l_2l_{C1}c\varphi_2)-m_{\mathrm{T}}(l_{\mathrm{p1}}^2+l_{\mathrm{p2}}^2-l_1^2+2l_1(l_{\mathrm{p1}}c\varphi_1-l_{\mathrm{p2}}s\varphi_1)+ \\ l_2(l_{\mathrm{p1}}c\varphi_{12}-l_{\mathrm{p2}}s\varphi_{12}+l_1c\varphi_2))-I_{\mathrm{T}}-I_1 \end{bmatrix},$$

$\left[\mathrm{M}(:,3)\right]=$

$$\begin{bmatrix} m_{\mathrm{T}}(l_{\mathrm{p1}}^2+l_{\mathrm{p2}}^2+l_2(l_{\mathrm{p1}}c\varphi_{12}-l_{\mathrm{p2}}s\varphi_{12})+l_1(l_{\mathrm{p1}}c\varphi_1-l_{\mathrm{p2}}s\varphi_1))+I_{\mathrm{T}} \\ \hline -m_1(l_{\mathrm{C1}}^2+l_2l_{C1}c\varphi_2)-m_{\mathrm{T}}(l_{\mathrm{p1}}^2+l_{\mathrm{p2}}^2-l_1^2+2l_1(l_{\mathrm{p1}}c\varphi_1-l_{\mathrm{p2}}s\varphi_1)+ \\ l_2(l_{\mathrm{p1}}c\varphi_{12}-l_{\mathrm{p2}}s\varphi_{12}+l_1c\varphi_2))-I_{\mathrm{T}}-I_1 \\ \hline I_{\mathrm{T}}+m_1(l_{\mathrm{C1}}^2+l_2^2+2l_2l_{C1}c\varphi_2)+m_2l_{\mathrm{C2}}^2+m_{\mathrm{T}}(l_{\mathrm{p1}}^2+l_{\mathrm{p2}}^2+l_2^2-l_1^2+ \\ 2l_1(l_{\mathrm{p1}}c\varphi_1-l_{\mathrm{p2}}s\varphi_1)+2l_2(l_{\mathrm{p1}}c\varphi_{12}-l_{\mathrm{p2}}s\varphi_{12}+l_1c\varphi_2))+I_1+I_2 \end{bmatrix},$$

where I_{T}, I_1, I_2 are the moments of inertia of the trunk, upper leg, lower leg, respectively, and m_1, m_2, m_{T} are the masses of the upper leg, lower leg and the trunk segment, respectively. Moments of inertia of the motors are neglected in the stance leg model.

The joints angular speed coupling matrix $\left[\mathrm{C}(\vec{\varphi}(t),\dot{\vec{\varphi}}(t))\right]$ is given by columns as follows

$\left[\mathrm{C}(:,1)\right]=$

$$\begin{bmatrix} k_{\mathrm{mh}} \\ m_{\mathrm{T}}l_1(\dot{\varphi}_{123}-\dot{\varphi}_{23})(l_{\mathrm{p1}}s\varphi_1+l_{\mathrm{p2}}c\varphi_1) \\ m_{\mathrm{T}}(l_2(2\dot{\varphi}_3-\dot{\varphi}_{12})(l_{\mathrm{p1}}s\varphi_{12}+l_{\mathrm{p2}}c\varphi_{12})+l_1\dot{\varphi}_3(l_{\mathrm{p1}}s\varphi_1+l_{\mathrm{p2}}c\varphi_1)) \end{bmatrix},$$

$\left[\mathrm{C}(:,2)\right]=$

$$\begin{bmatrix} m_{\mathrm{T}}l_1(\dot{\varphi}_2-2\dot{\varphi}_3)(l_{\mathrm{p1}}s\varphi_1+l_{\mathrm{p2}}c\varphi_1) \\ \hline k_{\mathrm{k}} \\ \hline (\dot{\varphi}_{23}-\dot{\varphi}_3)s\varphi_2(m_1l_2l_{\mathrm{C1}}+m_{\mathrm{T}}l_2l_1)s\varphi_2+m_{\mathrm{T}}(l_1\dot{\varphi}_{23}(l_{\mathrm{p1}}s\varphi_1+ \\ l_{\mathrm{p2}}c\varphi_1)+l_2(\dot{\varphi}_{12}-2\dot{\varphi}_3)(l_{\mathrm{p1}}s\varphi_{12}+l_{\mathrm{p2}}c\varphi_{12}) \end{bmatrix},$$

$\left[\mathrm{C}(:,3)\right]=$

$$\begin{bmatrix} m_{\mathrm{T}}\dot{\varphi}_3(l_2(l_{\mathrm{p1}}s\varphi_1+l_{\mathrm{p2}}c\varphi_1)+l_1(l_{\mathrm{p1}}s\varphi_{12}+l_{\mathrm{p2}}c\varphi_{12})) \\ \dot{\varphi}_3l_2(m_{\mathrm{T}}(l_{\mathrm{p1}}s\varphi_{12}+l_{\mathrm{p2}}c\varphi_{12})+(m_1l_{\mathrm{C1}}+m_{\mathrm{T}}l_1)s\varphi_2) \\ k_{\mathrm{ma}} \end{bmatrix},$$

where k_{mh}, k_{k} and k_{ma} are the effective damping coefficients for the hip, knee and ankle joints, respectively.